




## Toward a Unified Description of Isoscalar Giant Monopole Resonances in a Self-Consistent Quasiparticle-Vibration Coupling Approach

Z. Z. Li (李征征)<sup>1,2,3</sup>, Y. F. Niu (牛一斐)<sup>1,2,\*</sup> and G. Colò<sup>3,4,†</sup>

<sup>1</sup>*School of Nuclear Science and Technology, Lanzhou University, Lanzhou 730000, China*

<sup>2</sup>*Frontiers Science Center for Rare Isotope, Lanzhou University, Lanzhou 730000, China*

<sup>3</sup>*Dipartimento di Fisica, Università degli Studi di Milano, via Celoria 16, 20133 Milano, Italy*

<sup>4</sup>*INFN sezione di Milano, via Celoria 16, 20133 Milano, Italy*



(Received 3 November 2022; revised 20 February 2023; accepted 7 July 2023; published 23 August 2023)

The nuclear incompressibility is a key parameter of the nuclear equation of state that can be extracted from the measurements of the so-called “breathing mode” of finite nuclei. The most serious discrepancy so far is between values extracted from Pb and Sn, that has provoked the longstanding question “Why is tin so soft?”. To solve this puzzle, a fully self-consistent quasiparticle random-phase approximation plus quasiparticle-vibration coupling approach based on Skyrme-Hartree-Fock-Bogoliubov is developed. We show that the many-body correlations introduced by quasiparticle-vibration coupling, which shift the isoscalar giant monopole resonance energy in Sn isotopes by about 0.4 MeV more than the energy in <sup>208</sup>Pb, play a crucial role in providing a unified description of the isoscalar giant monopole resonance in Sn and Pb isotopes. The best description of the experimental strength functions is given by SV-K226 and KDE0, which are characterized by incompressibility values  $K_\infty = 226$  MeV and 229 MeV, respectively, at mean field level.

DOI: 10.1103/PhysRevLett.131.082501

The nuclear equation of state (EOS) represents the energy per nucleon,  $E/A$ , as a function of the neutron and proton densities of a uniform system. It is a fundamental ingredient for the description of heavy-ion collision dynamics, nuclear structure, static and dynamical properties of neutron stars, core-collapse supernova, and binary compact-star mergers [1–4]. The nuclear incompressibility  $K_\infty$  is a key parameter of the EOS related to the curvature of  $E/A$  of symmetric nuclear matter around its minimum,  $\rho_0$ , by  $K_\infty = 9\rho_0^2[(d^2/d\rho^2)(E/A)]_{\rho=\rho_0}$ . The nuclear compression-mode resonances, especially the “breathing mode” of finite nuclei, i.e., isoscalar giant monopole resonance (ISGMR), are a unique probe for the nuclear incompressibility  $K_\infty$  [5–7]. A key issue, as we discuss in what follows, is how to get a unified description of ISGMR strength functions in different isotopic chains, and determine  $K_\infty$  accurately without an uncontrolled nucleus dependence.

In <sup>208</sup>Pb, the ISGMR was measured in the Research Center for Nuclear Physics (RCNP, Osaka University) by means of inelastic  $\alpha$  scattering [8,9] and inelastic deuteron scattering [10], and in Texas A&M University (TAMU) by means of inelastic  $\alpha$  scattering [11,12]. These measurements, together with those performed in <sup>90</sup>Zr [9,13,14], hint to a value  $K_\infty = 240 \pm 20$  MeV for the nuclear incompressibility [7]. However, it was found that in even-even stable tin isotopes, <sup>112–124</sup>Sn, the ISGMR centroid energy is overestimated (by about 1 MeV) by the same models which reproduce the ISGMR centroid energy well in

<sup>208</sup>Pb [15,16]. This means that the incompressibility value that is deduced from Sn is lower than the one deduced from Pb or, in other words, the EOS is softer [17–19]. Later, a similar “softness” was also found in even-even <sup>106,110–116</sup>Cd isotopes [20] and even-even <sup>94–100</sup>Mo isotopes [21].

In the present work, we want to address the question “Why is tin so soft?” in a novel manner. In the papers we have mentioned, the correspondence between  $K_\infty$  and the ISGMR energy is established by means of quasiparticle random-phase approximation (QRPA) calculations. QRPA is a well-known microscopic method that describes giant resonances (GRs) as coherent superpositions of two-quasiparticle states. The axial deformation within the QRPA model helps to explain the softness in Mo isotopes [22], but tin nuclei are spherical. A lot of effort has been devoted to exploring the effects of nuclear superfluidity that show up in open-shell nuclei, namely pairing effects, within the self-consistent QRPA model [23–25]. It has been shown that surface pairing can partly reconcile tin and lead results (compared to volume pairing and mixed pairing) [23,24]. However, there is no strong argument on which type of pairing force should be favored over others. Moreover, the proposed “mutually enhanced magicity” effect on nuclear incompressibility, that is another attempt to solve the Sn-Pb puzzle, has also been ruled out by the measurement in <sup>204,206</sup>Pb [8,26].

Despite the big successes achieved in QRPA, the widths, decay properties, and fine structures of GRs are not well

described in QRPA because of the lack of coupling with more complex configurations than the two-quasiparticle ones. The particle-vibration coupling (PVC) effects have been proven to be crucial for reproducing the widths [27] and describing the decay properties of GRs [28]. These PVC effects have been included in a self-consistent way, based on both nonrelativistic density functional theory [29–33] and relativistic density functional theory [34–36]. Although many works have been devoted, e.g., to the electric dipole resonances [29,36–38] within the quasiparticle-vibration coupling framework, this is not the case for the ISGMR.

In this Letter, a fully self-consistent quasiparticle random-phase approximation plus quasiparticle-vibration coupling model (QPVC) is developed, based on the Skyrme-Hartree-Fock-Bogoliubov framework. In it, we consider both QPVC effects and pairing effects self-consistently. We give a short description of our framework, and more details will be discussed in a forthcoming publication. We aim to demonstrate that the consideration of QPVC effects is crucial in order to reach a unified description of the ISGMR in Sn, Pb, and also in the Ca isotopes that have been recently measured.

We start from the spherical Skyrme-Hartree-Fock-Bogoliubov code in the coordinate space from Ref. [39]. The so-called volume pairing force,  $v_{pp}(\mathbf{r}_1, \mathbf{r}_2) = V_{0,q}\delta(\mathbf{r}_1 - \mathbf{r}_2)$ , is used to describe the pairing interaction, where  $q$  labels either neutrons or protons.  $V_{0,q}$  is adjusted by fitting the pairing gaps according to the five-point formula [40]. The QRPA equations are solved in the canonical basis. The spurious state, caused by the violation of particle number, is removed as in Ref. [23]. On top of QRPA, we have included the coupling with phonons having  $J^\pi = 0^+, 1^-, 2^+, 3^-, 4^+$ , and  $5^-$  with energy less than 30 MeV and exhausting a fraction of non-energy-weighted (isoscalar or isovector) sum rule larger than 2%. The subtraction procedure is adopted, as described in [41]. Further numerical details are provided in Supplemental Material [42], where we also show that the final numerical results are stable with respect to the choice of the model space.

The sum rules, or  $k$ -th moments of the strength function  $S(E)$  are defined as  $m_k = \int_0^\infty S(E)E^k dE$ . In our case,  $S(E)$  is with respect to the operator  $\hat{F}_{00} = \sum_{i=1}^A r_i^2$ . The fulfillment of the energy-weighted sum rule  $m_1$  (%), and inverse energy-weighted sum rule  $m_{-1}$  ( $\text{fm}^4/\text{MeV}$ ), calculated by QRPA + QPVC, have been checked (see Supplemental Material [42]). There are many choices of characteristic energy for GRs, such as the centroid energy  $m_1/m_0$ , the constrained energy  $\sqrt{m_1/m_{-1}}$ , and the scaling energy  $\sqrt{m_3/m_1}$ . In the following, we will use the constrained energy  $\sqrt{m_1/m_{-1}}$  for our discussion since  $m_{-1}$  is unchanged in the case of QPVC with subtraction. Our conclusions would remain the same if we were to choose

another definition for the ISGMR energy. The ISGMR energies are calculated in the energy interval 10–30 MeV for Ca, and 5–25 MeV for Sn and Pb, because the strength is negligible outside these intervals.

In Fig. 1, we show the strength functions of the ISGMR, obtained either in the framework of (Q)RPA by using a smoothing with Lorentzians having a width of 1 MeV [dash-dotted (black) line], or within (Q)RPA + (Q)PVC [solid (blue) line], using the SV-K226 Skyrme force, in the even-even  $^{112-124}\text{Sn}$ ,  $^{48}\text{Ca}$ , and  $^{208}\text{Pb}$  nuclei. We compare the results with the experimental ones [(green) crosses] [8,15,45]. In general, with the inclusion of (Q)PVC effects, the results are significantly improved with respect to (Q)RPA, so we can achieve a good description of data both in the light  $^{48}\text{Ca}$  isotope, medium-heavy Sn isotopes, and heavy  $^{208}\text{Pb}$ . In  $^{112-124}\text{Sn}$ , QRPA gives one small peak and one higher peak while the experimental strength displays a broad single peak. The ISGMR energies are higher than the experimental ones, as pointed out in previous papers [17,19]. With the inclusion of QPVC effects, widths are comparable with the experimental ones (cf. also [46]). Moreover, within the self-consistent QRPA + QPVC model, the downward shifts of energies by 0.7–0.8 MeV (with respect to QRPA) make the ISGMR energies in agreement with data, along the whole Sn isotopic chain. In the case of  $^{48}\text{Ca}$ , the strength function has two main peaks in the RPA calculation, while the experimental strength shows only a single main peak. With PVC effects, the first peak is slightly moved to lower energy, and the second peak becomes fragmented, making the results closer to experiment. In the case of  $^{208}\text{Pb}$ , the ISGMR energy given by RPA agrees with the experimental one. With PVC effects, the ISGMR has a very small shift to lower energy, and a larger width that again makes the result closer to the experiment finding.

In Fig. 2, the energy shifts of the ISGMR from (Q)RPA to (Q)RPA + (Q)PVC (considering  $E_c = \sqrt{m_1/m_{-1}}$ ) are given in even-even  $^{40-44,48}\text{Ca}$ ,  $^{112-124}\text{Sn}$ , and  $^{208}\text{Pb}$  isotopes using seven Skyrme parameter sets: SAMi (black square), SkM\* (red circle), SkP (up blue triangle), SV-K226 (green diamond), SV-K241 (left navy blue triangle), SV-bas (right violet triangle), and KDE0 (purple hexagon). These forces are obtained by different groups, using quite different fitting protocols, and span a large range of  $K_\infty$  from 201 to 245 MeV. As shown in Fig. 2, the energy shifts from (Q)RPA to (Q)RPA + (Q)PVC are less than 1 MeV in general. In detail, the results depend on the Skyrme set that is used, and the associated dispersion in the Sn isotopes is about 0.5 MeV. However, from Ca, Sn, to Pb, the energy shifts become smaller. The energy shifts in Ca and Sn isotopes are about 0.4 MeV larger than the ones in  $^{208}\text{Pb}$ , and this makes it possible to describe well the ISGMR in these different isotopes at the same time.

In the medium-heavy systems, the QRPA produces a dominant peak and the shift of that peak, induced by

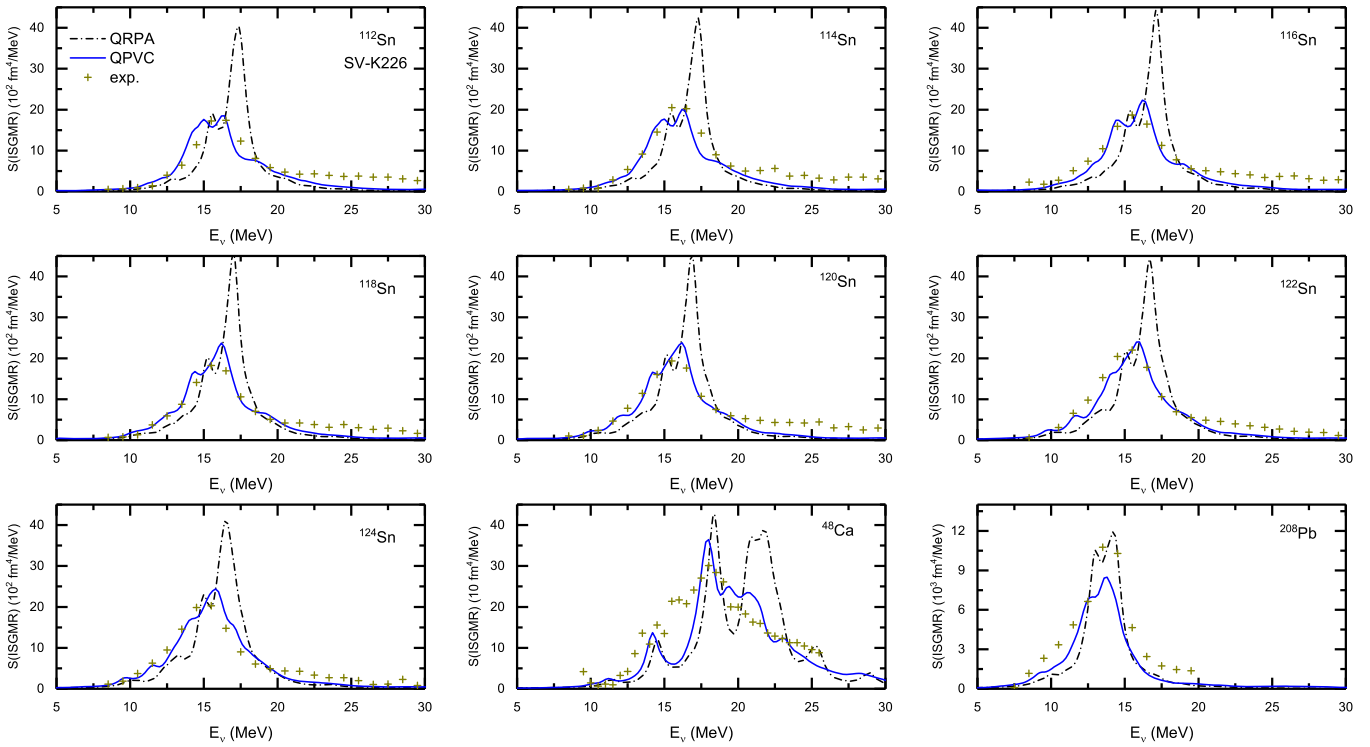


FIG. 1. ISGMR strength functions in even-even  $^{112-124}\text{Sn}$ ,  $^{48}\text{Ca}$ , and  $^{208}\text{Pb}$  isotopes, calculated either by (Q)RPA using a smoothing with Lorentzian having a width of 1 MeV [dash-dotted (black) line], or (Q)RPA + (Q)PVC [solid (blue) line]. The SV-K226 Skyrme force is used. The experimental data are given by green crosses [8,15,45].

QPVC, is essentially associated with its self-energy. The real part of the self-energy is, generally speaking, a negative quantity that decreases as a function of energy. However, when the energy is close to that of the two-quasiparticle

plus phonon energies, the self-energy may display a pole-like behavior and the overall trend changes. Therefore, the value of the self-energy and of the associated QPVC shift is essentially ruled by the relative position of the ISGMR and of the two-quasiparticle plus phonon states to which it is coupled. The presence or absence of pairing, and the resulting effect on the two-quasiparticle energies, explain the difference between the energy shifts in Sn isotopes and  $^{208}\text{Pb}$ . Detailed figures and estimates are provided in Supplemental Material [42], where we also discuss the case of Ca isotopes which, however, is more complicated because there is not only one dominant QRPA peak. In fact, one can notice that the QPVC effects in the magic  $^{40,48}\text{Ca}$  isotopes are larger than that in the open-shell nuclei  $^{42,44}\text{Ca}$  in most cases. This different behavior between open-shell and closed-shell Ca isotopes can also be, to some extent, understood by the change in the energy difference between two-quasiparticle plus phonon states and the ISGMR, as the two-quasiparticles states are affected by the pairing gap.

The linear correlation between the ISGMR energies and  $K_\infty$ , calculated by different models, is often used as a way to constrain  $K_\infty$  [47]. Therefore, in principle, one can expect a linear correlation between the ISGMR energies in different nuclei. In the upper panel of Fig. 3, we show that there is a linear correlation between the ISGMR energies in  $^{120}\text{Sn}$  and  $^{208}\text{Pb}$ , both in the (Q)RPA case (black square) and in the (Q)PVC case (blue circle). We use the seven Skyrme

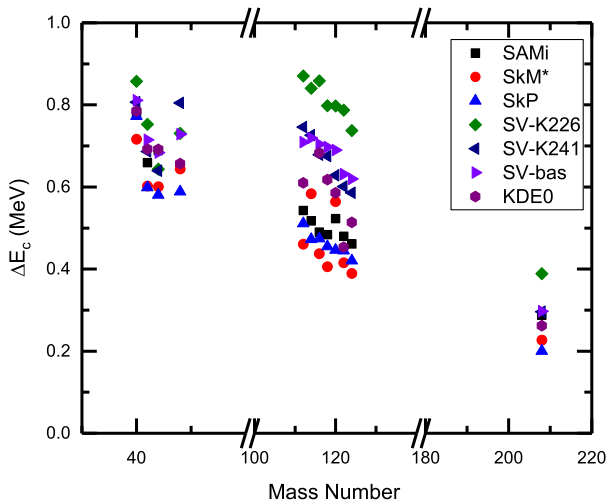


FIG. 2. The energy shifts of ISGMR from (Q)RPA to (Q)RPA + (Q)PVC ( $E_c = \sqrt{m_1/m_{-1}}$ ) in even-even  $^{40-44,48}\text{Ca}$ ,  $^{112-124}\text{Sn}$ , and  $^{208}\text{Pb}$  isotopes with seven Skyrme sets: SAMi (black square), SkM\* (red circle), SkP (up blue triangle), SV-K226 (green diamond), SV-K241 (left navy blue triangle), SV-bas (right violet triangle), and KDE0 (purple hexagon).

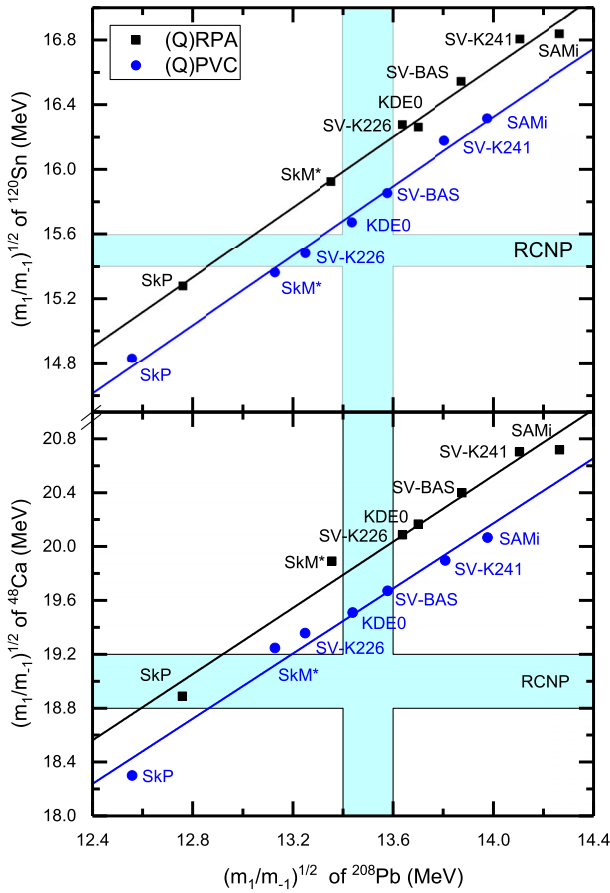


FIG. 3. The ISGMR energies in  $^{208}\text{Pb}$  vs the ones in  $^{120}\text{Sn}$  (upper panel), and  $^{48}\text{Ca}$  (lower panel). These are calculated by (Q)RPA (black square), and by (Q)RPA + (Q)PVC (blue circle) using seven different Skyrme parameters. The regression lines are obtained by a least-square linear fit of the (Q)RPA results and (Q)RPA + (Q)PVC results, respectively. The experimental data and their uncertainties, taken from [8,15,48], are displayed by means of cyan-colored bands.

interactions that we have already mentioned. The regression lines are obtained by a least-square fit. For the calculations in  $^{120}\text{Sn}$ , the volume pairing interaction is adopted. In the lower panel of Fig. 3, the same kind of linear correlation, between the ISGMR energies in  $^{48}\text{Ca}$  and  $^{208}\text{Pb}$ , is presented. The experimental data and their uncertainties are taken from [8,15,48]. The interesting point is that one cannot describe the ISGMR energy of  $^{120}\text{Sn}$  (or  $^{48}\text{Ca}$ ) and  $^{208}\text{Pb}$  simultaneously at the QRPA level, since the regression line is far from the crossing zone of experimental bands for these two nuclei. For example, SV-K226 and KDE0 give a good description in  $^{208}\text{Pb}$ , but they overestimate the ISGMR energy in  $^{120}\text{Sn}$  by about 0.8 MeV. However, with the consideration of (Q)PVC effects, the regression line given by the QPVC results is shifted downward by about 0.3 MeV, so it is marginally compatible with the experimental zone. In this case, SV-K226 and KDE0 give pretty good ISGMR energies

TABLE I. The deviation of ISGMR energies from experimental data [ $|E_c^{\text{theo}} - E_c^{\text{exp}}|$  (MeV)] in  $^{48}\text{Ca}$ ,  $^{120}\text{Sn}$ , and  $^{208}\text{Pb}$ , calculated by (Q)RPA and (Q)RPA + (Q)PVC using the Skyrme parameter sets SkP, SkM\*, SV-K226, KDE0, SV-bas, SV-K241, and SAMi. The experimental data are taken from [8,15,48].

	SkP	SkM*	SV-K226	KDE0	SV-bas	SV-K241	SAMi
$K_\infty$	201	217	226	229	233	241	245
(Q)RPA							
$^{48}\text{Ca}$	0.11	0.89	1.09	1.17	1.40	1.70	1.72
$^{120}\text{Sn}$	0.22	0.43	0.78	0.76	1.05	1.31	1.34
$^{208}\text{Pb}$	0.74	0.14	0.14	0.20	0.37	0.60	0.76
(Q)PVC							
$^{48}\text{Ca}$	0.70	0.25	0.36	0.51	0.67	0.90	1.07
$^{120}\text{Sn}$	0.67	0.14	0.02	0.18	0.36	0.68	0.82
$^{208}\text{Pb}$	0.94	0.37	0.25	0.06	0.08	0.31	0.48

in both  $^{120}\text{Sn}$  and  $^{208}\text{Pb}$ . The same conclusion is achieved looking at  $^{48}\text{Ca}$  and  $^{208}\text{Pb}$ , as shown in the lower panel. In the latter case, PVC effects play a unique role since there is no pairing. In summary, our results suggest that the (Q)PVC effects are crucial in order to reach a unified description of the ISGMR in Ca, Sn, and Pb isotopes.

The constraint on  $K_\infty$  is less clear in the theories beyond mean field, because it is hard to calculate  $K_\infty$  due to the ultraviolet divergence associated with zero-range effective interactions [49]. Nevertheless, with the subtraction procedure, we can assume that  $K_\infty$  will be the same as that at the mean field level [41,50]. The deviations of ISGMR energies from experimental data [ $|E_c^{\text{theo}} - E_c^{\text{exp}}|$  (MeV)] in  $^{48}\text{Ca}$ ,  $^{120}\text{Sn}$ , and  $^{208}\text{Pb}$  are given in Table I, calculated by (Q)RPA and (Q)RPA + (Q)PVC using SkP, SkM\*, SV-K226, KDE0, SV-bas, SV-K241, and SAMi. The table shows that, at (Q)RPA level,  $^{48}\text{Ca}$  and  $^{120}\text{Sn}$  prefer SkP with a small incompressibility,  $K_\infty = 201$  MeV. However,  $^{208}\text{Pb}$  prefers SkM\*, SV-K226, and KDE0, with  $K_\infty$  ranging from 217 to 229 MeV. With the inclusion of (Q)PVC effects,  $^{48}\text{Ca}$  prefers SkM\* and SV-K226,  $^{120}\text{Sn}$  prefers SkM\*, SV-K226, and KDE0, while  $^{208}\text{Pb}$  prefers SV-K226, KDE0, and SV-bas. Thus, SV-K226 and KDE0 describe all three nuclei very well at the same time, with  $K_\infty = 226$  MeV and 229 MeV, respectively: this is consistent with the constraint  $240 \pm 20$  MeV, obtained previously from the ISGMR of  $^{208}\text{Pb}$  in QRPA [7].

In summary, we have developed a fully self-consistent approach, that is, a QRPA plus QPVC model, based on Skyrme-Hartree-Fock-Bogoliubov. We have clearly demonstrated that the inclusion of QPVC effects is crucial in order to achieve a unified description of the ISGMR in Ca, Sn, and Pb isotopes at the same time. The so-called softness of Sn isotopes is explained then, to a large extent, by the effects induced by QPVC. SV-K226 and KDE0 are found

to give the best description of the experimental strength functions.

We should add that (Q)PVC only accounts for the  $2p$ - $2h$  (or  $4qp$ ) configurations, and more complex configurations are missing. A theory that goes beyond may further improve the agreement with experimental data in different mass regions. It is also important, in a future investigation, to study the pattern of the energy shifts for giant resonances with different multipolarities, as well as the possible impact on EOS parameters. This can be done using the newly developed, fully self-consistent model that we have just introduced.

This research was partly supported by the National Key Research and Development (R&D) Program under Grant No. 2021YFA1601500 and Natural Science Foundation of China under Grant No. 12075104. Z. L. acknowledges the support by China Scholarship Council (CSC) under Grant No. 202106180051.

*Note added.*—During the referral process, a work by Litvinova [51] has been become available. This deals with the topic of the current work, and confirms the relevance of QPVC correlations.

\* niuyf@lzu.edu.cn

† gianluca.colò@mi.infn.it

- [1] X. Roca-Maza and N. Paar, *Prog. Part. Nucl. Phys.* **101**, 96 (2018).
- [2] G. F. Burgio, H.-J. Schulze, I. Vidaña, and J.-B. Wei, *Prog. Part. Nucl. Phys.* **120**, 103879 (2021).
- [3] M. Oertel, M. Hempel, T. Klähn, and S. Typel, *Rev. Mod. Phys.* **89**, 015007 (2017).
- [4] A. Perego, D. Logoteta, D. Radice, S. Bernuzzi, R. Kashyap, A. Das, S. Padamata, and A. Prakash, *Phys. Rev. Lett.* **129**, 032701 (2022).
- [5] M. N. Harakeh and A. Woude, *Giant Resonances: Fundamental High-Frequency Modes of Nuclear Excitation* (Clarendon Press, Oxford, 2001), Vol. 24.
- [6] J. Blaizot, *Phys. Rep.* **64**, 171 (1980).
- [7] U. Garg and G. Colò, *Prog. Part. Nucl. Phys.* **101**, 55 (2018).
- [8] D. Patel, U. Garg, M. Fujiwara, T. Adachi, H. Akimune, G. Berg, M. Harakeh, M. Itoh, C. Iwamoto, A. Long, J. Matta, T. Murakami, A. Okamoto, K. Sault, R. Talwar, M. Uchida, and M. Yosoi, *Phys. Lett. B* **726**, 178 (2013).
- [9] M. Uchida, H. Sakaguchi, M. Itoh, M. Yosoi, T. Kawabata, Y. Yasuda, H. Takeda, T. Murakami, S. Terashima, S. Kishi, U. Garg, P. Boutachkov, M. Hedden, B. Kharraja, M. Koss, B. K. Nayak, S. Zhu, M. Fujiwara, H. Fujimura, H. P. Yoshida, K. Hara, H. Akimune, and M. N. Harakeh, *Phys. Rev. C* **69**, 051301(R) (2004).
- [10] D. Patel, U. Garg, M. Itoh, H. Akimune, G. Berg, M. Fujiwara, M. Harakeh, C. Iwamoto, T. Kawabata, K. Kawase, J. Matta, T. Murakami, A. Okamoto, T. Sako, K. Schlax, F. Takahashi, M. White, and M. Yosoi, *Phys. Lett. B* **735**, 387 (2014).
- [11] D. H. Youngblood, H. L. Clark, and Y.-W. Lui, *Phys. Rev. Lett.* **82**, 691 (1999).
- [12] D. H. Youngblood, Y.-W. Lui, H. L. Clark, B. John, Y. Tokimoto, and X. Chen, *Phys. Rev. C* **69**, 034315 (2004).
- [13] Krishichayan, Y.-W. Lui, J. Button, D. H. Youngblood, G. Bonasera, and S. Shlomo, *Phys. Rev. C* **92**, 044323 (2015).
- [14] Y. Gupta, U. Garg, K. Howard, J. Matta, M. Senyigit, M. Itoh, S. Ando, T. Aoki, A. Uchiyama, S. Adachi, M. Fujiwara, C. Iwamoto, A. Tamii, H. Akimune, C. Kadono, Y. Matsuda, T. Nakahara, T. Furuno, T. Kawabata, M. Tsumura, M. Harakeh, and N. Kalantar-Nayestanaki, *Phys. Lett. B* **760**, 482 (2016).
- [15] T. Li *et al.*, *Phys. Rev. Lett.* **99**, 162503 (2007).
- [16] T. Li *et al.*, *Phys. Rev. C* **81**, 034309 (2010).
- [17] J. Piekarewicz, *Phys. Rev. C* **76**, 031301(R) (2007).
- [18] J. Piekarewicz, *J. Phys. G* **37**, 064038 (2010).
- [19] U. Garg *et al.*, *Nucl. Phys.* **A788**, 36 (2007).
- [20] D. Patel, U. Garg, M. Fujiwara, H. Akimune, G. Berg, M. Harakeh, M. Itoh, T. Kawabata, K. Kawase, B. Nayak, T. Ohta, H. Ouchi, J. Piekarewicz, M. Uchida, H. Yoshida, and M. Yosoi, *Phys. Lett. B* **718**, 447 (2012).
- [21] K. Howard *et al.*, *Phys. Lett. B* **807**, 135608 (2020).
- [22] G. Colò, D. Gambacurta, W. Kleinig, J. Kvasil, V. O. Nesterenko, and A. Pastore, *Phys. Lett. B* **811**, 135940 (2020).
- [23] J. Li, G. Colò, and J. Meng, *Phys. Rev. C* **78**, 064304 (2008).
- [24] L.-G. Cao, H. Sagawa, and G. Colò, *Phys. Rev. C* **86**, 054313 (2012).
- [25] P. Avogadro and C. A. Bertulani, *Phys. Rev. C* **88**, 044319 (2013).
- [26] E. Khan, *Phys. Rev. C* **80**, 057302 (2009).
- [27] G. F. Bertsch, P. F. Bortignon, and R. A. Broglia, *Rev. Mod. Phys.* **55**, 287 (1983).
- [28] W. L. Lv, Y. F. Niu, and G. Colò, *Phys. Rev. C* **103**, 064321 (2021).
- [29] N. Lyutorovich, V. I. Tselyaev, J. Speth, S. Krewald, F. Grümmer, and P.-G. Reinhard, *Phys. Rev. Lett.* **109**, 092502 (2012).
- [30] N. Lyutorovich, V. Tselyaev, J. Speth, S. Krewald, F. Grümmer, and P.-G. Reinhard, *Phys. Lett. B* **749**, 292 (2015).
- [31] V. Tselyaev, N. Lyutorovich, J. Speth, S. Krewald, and P.-G. Reinhard, *Phys. Rev. C* **94**, 034306 (2016).
- [32] X. Roca-Maza, Y. F. Niu, G. Colò, and P. Bortignon, *J. Phys. G* **44**, 044001 (2017).
- [33] Y. F. Niu, G. Colò, E. Vigezzi, C. L. Bai, and H. Sagawa, *Phys. Rev. C* **94**, 064328 (2016).
- [34] E. Litvinova, P. Ring, and V. Tselyaev, *Phys. Rev. C* **75**, 064308 (2007).
- [35] E. Litvinova, P. Ring, and D. Vretenar, *Phys. Lett. B* **647**, 111 (2007).
- [36] E. Litvinova, P. Ring, and V. Tselyaev, *Phys. Rev. C* **78**, 014312 (2008).
- [37] I. A. Egorova and E. Litvinova, *Phys. Rev. C* **94**, 034322 (2016).
- [38] A. Avdeenkov, S. Goriely, S. Kamedzhiev, and S. Krewald, *Phys. Rev. C* **83**, 064316 (2011).
- [39] K. Bennaceur and J. Dobaczewski, *Comput. Phys. Commun.* **168**, 96 (2005).

- [40] M. Bender, K. Rutz, P. G. Reinhard, and J. A. Maruhn, *Eur. Phys. J. A* **8**, 59 (2000).
- [41] V. I. Tselyaev, *Phys. Rev. C* **75**, 024306 (2007).
- [42] See Supplemental Material at <http://link.aps.org/supplemental/10.1103/PhysRevLett.131.082501> for details. It presents numerical inputs for calculations, check of sum rules, stability of the QPVC results, the description of  $^{90}\text{Zr}$ , and the mechanism underlying the QPVC shifts, which includes Refs. [43,44].
- [43] S. Shen, G. Colò, and X. Roca-Maza, *Phys. Rev. C* **101**, 044316 (2020).
- [44] Y. K. Gupta *et al.*, *Phys. Rev. C* **97**, 064323 (2018).
- [45] S. D. Olorunfunmi *et al.*, *Phys. Rev. C* **105**, 054319 (2022).
- [46] V. Tselyaev, J. Speth, S. Krewald, E. Litvinova, S. Kamedzhiev, N. Lyutorovich, A. Avdeenkov, and F. Grümmer, *Phys. Rev. C* **79**, 034309 (2009).
- [47] J. Blaizot, J. Berger, J. Dechargé, and M. Girod, *Nucl. Phys. A* **591**, 435 (1995).
- [48] K. Howard *et al.*, *Phys. Lett. B* **801**, 135185 (2020).
- [49] K. Moghrabi, M. Grasso, G. Colò, and N. Van Giai, *Phys. Rev. Lett.* **105**, 262501 (2010).
- [50] D. Gambacurta, M. Grasso, and J. Engel, *Phys. Rev. C* **92**, 034303 (2015).
- [51] E. Litvinova, *Phys. Rev. C* **107**, L041302 (2023).